Journal of Power Sources 183 (2008) 133–142

Contents lists available at ScienceDirect

Journal of Power Sources

journal homepage: www.elsevier.com/locate/jpowsour

Modeling of methane fed solid oxide fuel cells: Comparison between proton conducting electrolyte and oxygen ion conducting electrolyte

Meng Ni*, Dennis Y.C. Leung, Michael K.H. Leung

Department of Mechanical Engineering, The University of Hong Kong, Pokfulam Road, Hong Kong, P.R. China

ARTICLE INFO

Article history:
Received 31 March 2008
Received in revised form 28 April 2008
Accepted 28 April 2008
Available online 4 May 2008

Keywords:
Solid oxide fuel cell (SOFC)
Proton conducting electrolyte
Methane steam reforming (MSR)
Water gas shift (WGS)
Triple-phase boundary (TPB)
Multi-component mass transfer

ABSTRACT

An electrochemical model was developed to study the methane (CH_4) fed solid oxide fuel cell (SOFC) using proton conducting electrolyte (SOFC-H) and oxygen ion conducting electrolyte (SOFC-O). Both the internal methane steam reforming (MSR) and water gas shift (WGS) reactions are considered in the model. Previous study has shown that the CH_4 fed SOFC-H had significantly better performance than the SOFC-O. However, the present study reveals that the actual performance of the CH_4 fed SOFC-H is considerably lower than the SOFC-O, partly due to higher ohmic overpotential of SOFC-H. It is also found that the CH_4 fed SOFC-H has considerably higher cathode concentration overpotential and lower anode concentration overpotential than the SOFC-O. The anode concentration overpotentials of the CH_4 fed SOFC-H and SOFC-O are found to decrease with increasing temperature, which is different from previous analyses on the H_2 fed SOFC. Therefore, high temperature is desirable for increasing the potential of the CH_4 fed SOFC. It is also found that there exist optimal electrode porosities that minimize the electrode total overpotentials. The analyses provided in this paper signify the difference between the CH_4 fed SOFC-H and SOFC-O. The model developed in this paper can be extended to 2D or 3D models to study the performance of practical SOFC systems.

© 2008 Elsevier B.V. All rights reserved.

1. Introduction

Solid oxide fuel cell (SOFC) has been identified as a promising clean energy technology for electricity generation [1–13]. The high operating temperature of SOFC provides several advantages: (1) electrochemical reactions take place at a fast rate, eliminating the need of expensive noble metal catalyst, and thus, SOFC is potentially cost-effective; (2) high temperature waste heat from SOFC is of high quality and can be recovered to achieve high energy conversion efficiency; (3) alternative fuels, such as methane, methanol, ethanol, etc., can be directly used as fuels for SOFC without the need of any external reforming processors. Due to its great prospect for clean energy generation, SOFC has received more and more attention and extensive research works have been done in recent years [14–19].

Conventional SOFCs are based on oxygen ion conducting electrolyte (SOFC-O), i.e. yittria-stabilized zirconia (YSZ), because of its high ionic conductivity and sufficient stability at high temperature. Both experimental and mathematical modeling studies have been performed to study the performance of SOFC-O fed with hydrogen or alternative fuels such as methane and ethanol [20–25]. Alternatively, an SOFC can be built with a proton conducting ceramic as its electrolyte (SOFC-H), such as $BaCeO_3$-based ceramics [26–28]. The use of proton conducting electrolyte in an SOFC-H is advantageous because complete fuel utilization is possible, as H_2O is produced in the cathode. For comparison, H_2O is produced in the anode of an SOFC-O, which in turn dilutes the concentration of H_2 at the anode and raises the issue of gas separation [27]. In case ammonia is used as a fuel, an SOFC-H has an additional advantage, as no harmful nitrogen oxide gas will be generated [29–31]. For comparison, nitrogen oxide may be formed in the anode chamber of an SOFC-O as oxygen ions transporting through the dense electrolyte may react with N_2 at the surface of the catalyst particles. More interestingly, previous thermodynamic analyses have reported that an SOFC-H fed with H_2 or alternative fuels have a higher theoretical efficiency than an SOFC-O [32–36]. The reason is generally due to a higher H_2 partial pressure at the anode of an SOFC-H than an SOFC-O, leading to higher Nernst potential. However, in the above-mentioned thermodynamic analyses, only Nernst potentials are considered and no overpotentials are included. Therefore, the previous thermodynamic analyses cannot reveal the actual performance of SOFC-H and SOFC-O. In order to quantify the actual performance of an SOFC and identify potential methods for performance improvement, detailed electrochemical modeling analyses are desired. In literature, there

* Corresponding author. Tel.: +852 2859 2811; fax: +852 2858 5415.
E-mail address: memni@graduate.hku.hk (M. Ni).

0378-7753/$ – see front matter © 2008 Elsevier B.V. All rights reserved.
doi:10.1016/j.jpowsour.2008.04.073

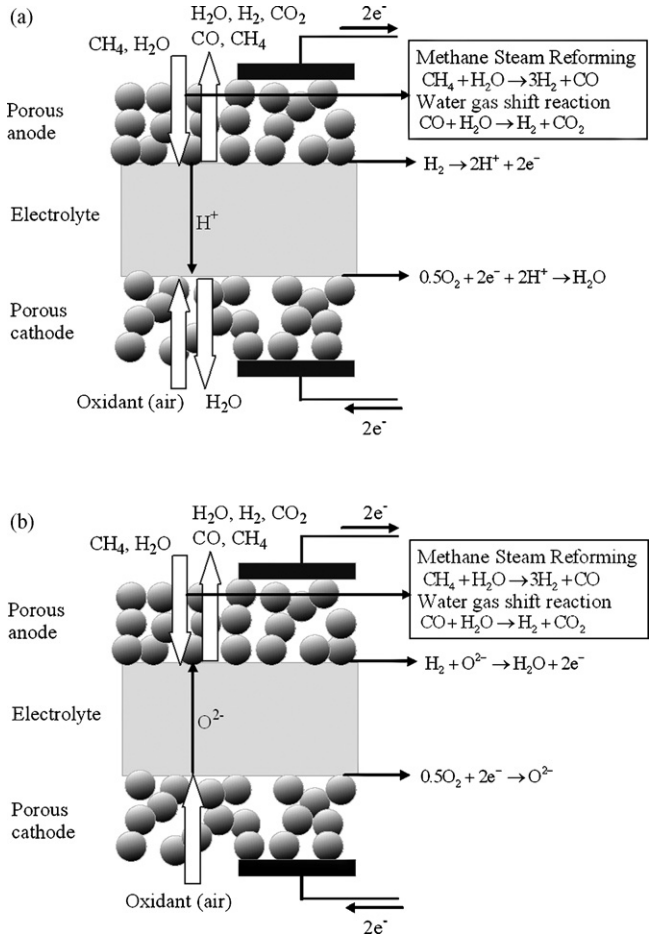

Fig. 1. Schematics of CH_4 fed SOFC (a) SOFC-H and (b) SOFC-O.

is only one study reporting the current density–voltage (J–V) characteristics of the SOFC-H fed with ethanol [37]. In that study, both activation overpotentials of the electrodes and ohmic overpotential of the electrolyte are considered but the concentration overpotentials are completely neglected. Ignoring the concentration loss can greatly simplify the electrochemical model; however, the important phenomena of transport and chemical reactions in the porous electrodes cannot be obtained. More importantly, such a simplification becomes invalid if the current density is sufficiently large because the concentration overpotential will be significant at high current density.

In this paper, a detailed electrochemical model has been developed to predict the performance of methane fed SOFC-H and SOFC-O. All possible voltage losses, i.e. activation overpotential, ohmic overpotential and concentration overpotential, are considered in the model. Detailed comparisons between SOFC-H and SOFC-O are made to better understand the working mechanisms of SOFC-H and SOFC-O and to identify key sources of voltage loss for further improvement.

2. Model development

The working mechanisms of the CH_4 fed SOFC-H and SOFC-O are illustrated in Fig. 1(a) and (b).

In the SOFC-H, methane–steam mixture and oxidant (air) are fed to the porous anode and cathode, respectively. In the anode, methane fuel undergoes direct internal methane steam reforming (MSR) to produce H_2 and CO on the surface of the catalyst particles

$$CH_4 + H_2O \leftrightarrow CO + 3H_2 \quad (1)$$

With sufficient H_2O, the produced CO can undergo water gas shift reaction (WGS) to produce CO_2 and additional H_2

$$CO + H_2O \leftrightarrow CO_2 + H_2 \quad (2)$$

The H_2 fuel produced travels through the porous anode to the triple-phase boundary (TPB) at the electrode–electrolyte interface, where the hydrogen molecules are electrochemically oxidized to produce protons and electrons. In addition to H_2, CO can also be electrochemically oxidized at the TPB. However, since the rate of CO conversion via WGS is much higher than the rate of its electrochemical reaction, the electrochemical oxidation of CO can be reasonably neglected [38–40]. In the cathode, the oxygen molecules are transported through the porous electrode layer to the TPB, where they react with the protons from the electrolyte and absorb the electrons from the external circuit to produce H_2O.

In the methane fed SOFC-O, the methane fuel undergoes similar MSR to produce H_2 and CO, which subsequently reacts with H_2O to produce additional H_2 via WGS. However, unlike SOFC-H, H_2O is only produced electrochemically at the anode for SOFC-O.

2.1. Working potential of the CH_4 fed SOFC-H

Considering all the overpotentials involved in the SOFC-H operation, the working potential (V) of CH_4 fed SOFC-H can be calculated as

$$V = E - \eta_{conc,a} - \eta_{conc,c} - \eta_{act,a} - \eta_{act,c} - \eta_{ohm} \quad (3)$$

where E, $\eta_{conc,a}$, $\eta_{conc,c}$, $\eta_{act,a}$, $\eta_{act,c}$, and η_{ohm} are the equilibrium voltage, anode concentration overpotential, cathode concentration overpotential, anode activation overpotential, cathode activation overpotential, and ohmic overpotential of the electrolyte, respectively.

2.1.1. Equilibrium voltage

It is well known that hydrogen oxidation in the porous anode is an electrochemical reaction process, while MSR and WGS are chemical reaction processes. Therefore, the equilibrium potential of the CH_4 fed SOFC can be calculated in terms of the partial pressures of the reactants/products of the electrochemical reaction according to the Nernst equation:

$$E = E_0 + \frac{RT}{2F} \ln\left(\frac{P_{H_2,a} P_{O_2,c}^{0.5}}{P_{H_2O,c}}\right) \quad (4)$$

where R is the universal gas constant (8.3145 J mol^{-1} K^{-1}); F is the Faraday constant (9.6485×10^7 C mol^{-1}); T is the absolute temperature (K); $P_{H_2,a}$, $P_{H_2O,c}$, and $P_{O_2,c}$ are the partial pressures of hydrogen, steam and oxygen, respectively. The subscripts a and c refer to the anode and cathode, respectively. The reversible potential (E_0) can be obtained from Ref. [41].

2.1.2. Concentration overpotential

The concentration overpotential measures the resistance of the porous structure to the transport of reactants approaching the reaction sites and the transport of products leaving the reaction sites. In a CH_4 fed SOFC-H, H_2 and O_2 are the reactants for the electrochemical reaction and H_2O generated in the cathode is the product. Therefore, the concentration overpotentials can be expressed in the Nernst form as

$$\eta_{conc,a} = \frac{RT}{2F} \ln\left(\frac{P_{H_2}}{P_{H_2}^{l}}\right) \quad (5)$$

and

$$\eta_{\text{conc,c}} = \frac{RT}{4F} \ln\left(\frac{P_{O_2}(P^{\text{l}}_{H_2O,c})^2}{P^{\text{l}}_{O_2}(P_{H_2O,c})^2}\right) \quad (6)$$

where $P^{\text{l}}_{H_2}$, $P^{\text{l}}_{O_2}$, and $P^{\text{l}}_{H_2O,c}$ represent the interfacial partial pressure of H_2 at the anode–electrolyte interface, partial pressure of O_2 at the cathode–electrolyte interface, and partial pressure of H_2O at the cathode–electrolyte interface, respectively. In order to determine the unknown interfacial partial pressure, the mass transport characteristics need to be determined.

2.1.2.1. Anode concentration overpotential. The reaction rates (mol m^{-3} s^{-1}) of MSR (R_{MSR}) and WGS (R_{WGS}) in the porous anode can be written as [42]:

$$R_{\text{MSR}} = k^{+}_{\text{MSR}} p_{CH_4} p_{H_2O} - k^{-}_{\text{MSR}} p_{CO} (p_{H_2})^3 \quad (7)$$

$$R_{\text{WGS}} = k^{+}_{\text{WGS}} p_{CO} p_{H_2O} - k^{-}_{\text{WGS}} p_{CO_2} p_{H_2} \quad (8)$$

where p are partial pressures (Pa); k are rate constants for reforming and shift reactions (mol m^{-3} Pa^{-2} s^{-1}); the superscripts + and − refers to the forward and backward reactions, respectively.

In a steady state, the transport of each participating component is determined by the local conservation of mass:

$$\frac{dN_{CH_4}}{dx} = -R_{\text{MSR}} \quad (9)$$

$$\frac{dN_{H_2O,a}}{dx} = -R_{\text{MSR}} - R_{\text{WGS}} \quad (10)$$

$$\frac{dN_{CO}}{dx} = R_{\text{MSR}} - R_{\text{WGS}} \quad (11)$$

$$\frac{dN_{H_2}}{dx} = 3R_{\text{MSR}} + R_{\text{WGS}} \quad (12)$$

$$\frac{dN_{CO_2}}{dx} = R_{\text{WGS}} \quad (13)$$

where N_i is the flux of species i (mol m^{-3} s^{-1}); x is the depth measured from electrode surface. The subscript a refers to the anode.

For modeling of multi-component gas transport in a porous medium, Fick's model (FM), Stefan–Maxwell model (SMM), and dusty gas model (DGM) are frequently used [43]. FM is the simplest model and is widely used in literature. However, FM assumes equimolar counter diffusion, which becomes invalid when the gas species have considerably different molecular weights. SMM relates the molar flux with molecular weights of gas species but neglects the effects of Knudsen diffusion. For comparison, DGM not only considers the effects of molecular weights of gas species, but also includes Knudsen flow mechanism. Comparisons between experiments and DGM simulation results have been conducted extensively and very good agreements have been obtained [43]. Therefore, in this study, DGM is selected to study the multi-component mass transfer within the porous SOFC electrodes. According to DGM, the transport of gas species i is governed by

$$\frac{N_i}{D^{\text{eff}}_{i,k}} + \sum_{j=1,j\neq i}^{n} \frac{y_j N_i - y_i N_j}{D^{\text{eff}}_{ij}} = -\frac{1}{RT}\left[P\frac{dy_i}{dx} + y_i\frac{dP}{dx}\left(1 + \frac{B_0 P}{D^{\text{eff}}_{i,k}\mu}\right)\right] \quad (14)$$

where y_i is the molar fraction of species i; $D^{\text{eff}}_{i,k}$ is the effective Knudsen diffusion coefficient of species i; D^{eff}_{ij} is the effective binary diffusion coefficient of species i and j; P is the local pressure inside the porous anode; B_0 is the permeability; and μ is the viscosity of gas mixture. The calculation procedures of the diffusion coefficients ($D^{\text{eff}}_{i,k}$ and D^{eff}_{ij}), viscosity, and permeability can be found elsewhere [44–46].

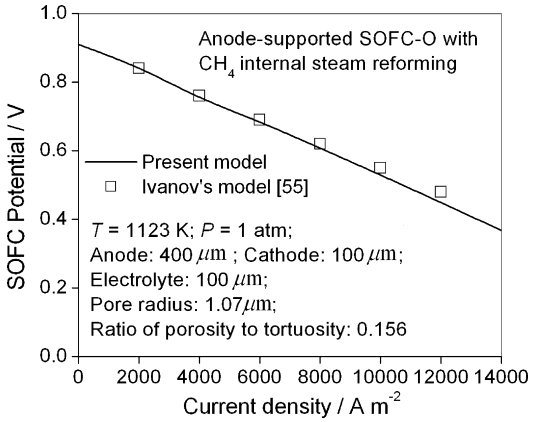

Fig. 2. Comparison between the present modeling results and literature data for model validation.

At the anode surface, the molar fractions of each species are known. At the electrode–electrolyte interface, electrochemical reactions take place and thus the flux of H_2 can be related with the current density as

$$N_{H_2}|_{x=d_a} = \frac{J}{2F} \quad (15)$$

where J is the current density (A m^{-2}) and d_a is the thickness of anode. As the remaining species are not involved in the electrochemical reaction, their fluxes at the electrode–electrolyte interface are equal to zero (i.e. $N_{H_2O,a}|_{x=d_a} = 0$; $N_{CH_4}|_{x=d_a} = 0$; $N_{CO}|_{x=d_a} = 0$; $N_{CO_2}|_{x=d_a} = 0$).

The above governing equations (Eqs. (9)–(14)) are inter-related differential equations and can be solved by numerical method. Finite difference method was used to discretize the governing equations. An iterative scheme was developed to obtain the solution at the discrete grids. After obtaining the molar fraction/partial pressure of each gas species inside the porous anode, the concentration overpotential at the SOFC-H anode can thus be calculated with Eq. (5).

2.1.2.2. Cathode concentration overpotential. In the cathode, O_2 is electrochemically consumed while H_2O is electrochemically produced and no chemical reaction is involved. Therefore, the transport

Table 1
Input parameters used in the mathematical model [42,49,57]

Parameter	Value
Temperature, T (K)	1073
Pressure, P (atm)	1.0
Coefficient of anode exchange current density, k_a	325
Coefficient of cathode exchange current density, k_c	1157
Activation energy for anode, $E_{act,a}$ (J mol^{-1})	1.0×10^5
Activation energy for cathode, $E_{act,c}$ (J mol^{-1})	1.2×10^5
Fuel composition (molar fraction) at the anode inlet	
CH_4 (%)	17.1
CO (%)	2.9
H_2O (%)	49.3
H_2 (%)	26.3
CO_2 (%)	4.4
Electrode porosity	0.4
Electrode tortuosity	5.0
Electrode pore radius (μm)	0.5
Anode thickness, d_a (μm)	500
Cathode thickness, d_c (μm)	50
Electrolyte thickness, d_e (μm)	50

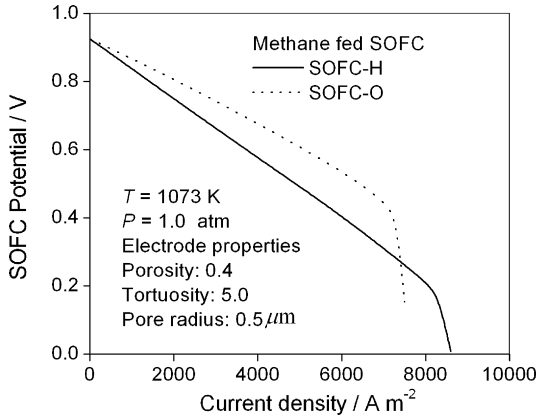

Fig. 3. Comparison of the operating voltage of SOFC-H and SOFC-O.

of gas species (O_2, N_2, and H_2O) can be determined by

$$\frac{dN_i}{dx} = 0 \quad (i = O_2,\ N_2,\ \text{and}\ H_2O) \tag{16}$$

The fluxes can be determined by the DGM (Eq. (14)). Similarly, molar fractions of gas species at the cathode surface are given. At the cathode–electrolyte interface, the fluxes of O_2 and H_2O can be related to the current density as

$$N_{O_2}|_{x=d_c} = \frac{J}{4F} \tag{17}$$

and

$$N_{H_2O,c}|_{x=d_c} = -\frac{J}{2F} \tag{18}$$

where d_c is the thickness of the cathode.

After solving the governing equations (Eq. (14)) with the above boundary conditions, the concentration overpotential at the cathode can be obtained from Eq. (6).

2.1.3. Activation overpotential

The activation overpotential is related to the electrode kinetics at the reaction site. The electrode activation overpotential–current density relationship can be expressed by the Butler–Volmer equation

$$J = J_0 \left[\exp\left(\frac{\alpha z F \eta_{act}}{RT}\right) - \exp\left(-\frac{(1-\alpha) z F \eta_{act}}{RT}\right)\right] \tag{19}$$

where J_0 is the exchange current density; z is the number of electrons involved per reaction; and α is the symmetrical factor. For a SOFC, the values of z and α are set to 2 and 0.5, respectively [47]. Therefore, the activation overpotentials of anode ($\eta_{act,a}$) and cathode ($\eta_{act,c}$) can be explicitly written as

$$\eta_{act,i} = \frac{RT}{F} \sinh^{-1}\left(\frac{J}{2J_{0,i}}\right) = \frac{RT}{F} \ln\left[\frac{J}{2J_{0,i}} + \sqrt{\left(\frac{J}{2J_{0,i}}\right)^2 + 1}\right], \quad i = a, c \tag{20}$$

where $J_{0,i}$ is the exchange current density that represents the readiness of an electrode to proceed with electrochemical reaction and

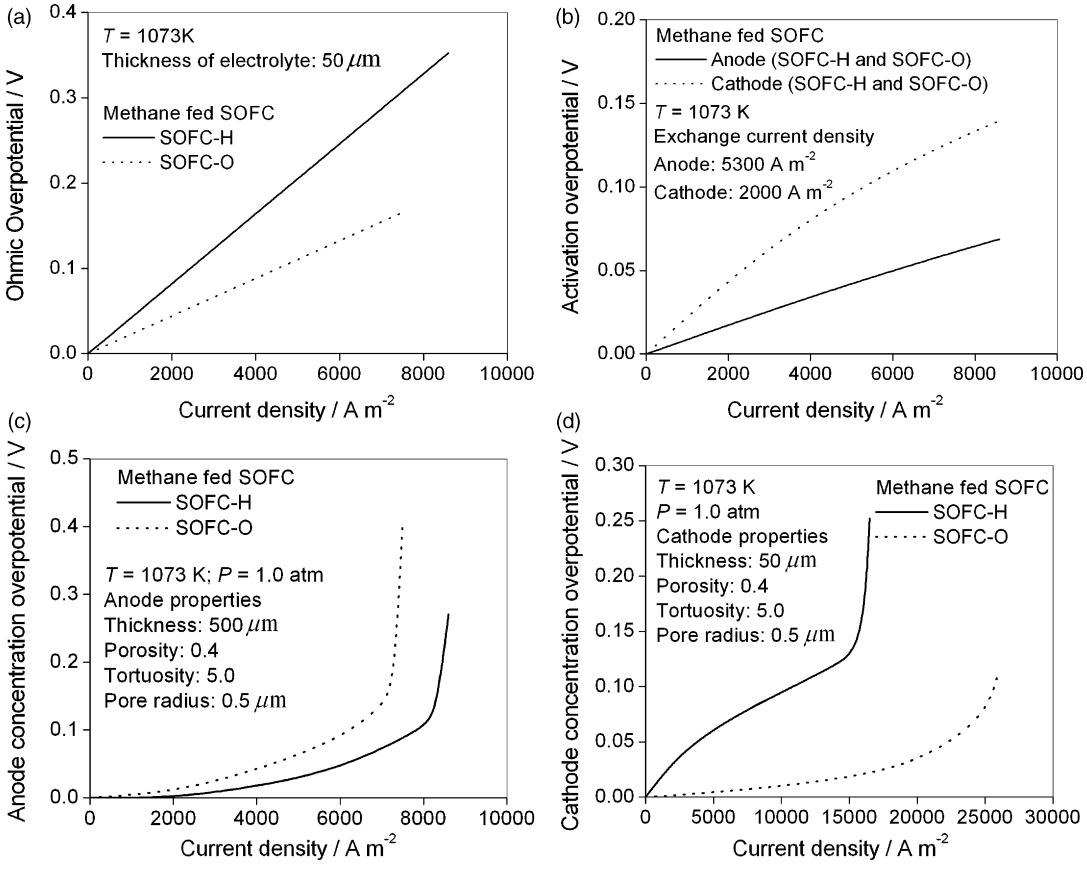

Fig. 4. Comparison of the overpotentials of CH_4 fed SOFC-H and SOFC-H: (a) Ohmic overpotential; (b) activation overpotential; (c) anode concentration overpotential; (d) cathode concentration overpotential.

the subscripts a and c represent anode and cathode, respectively [48]. The value of $J_{0,i}$ is proportional to the length of TPB, which represents the number of electrochemically active sites [49–52]

$$J_{0,i} \propto L_{TPB} \tag{21}$$

Previous analyses have shown that the TPB length is related to the electrode porosity (ε) and the pore radius (r_p) [50–52]

$$L_{TPB} \propto \frac{1-\varepsilon}{r_p} \tag{22}$$

In addition to the TPB length, operating temperature is also an important factor governing the exchange current density. Including the effects of both TPB length and operating temperature, the exchange current density can be expressed as

$$J_{0,a} = k_a \frac{1-\varepsilon}{r_p} \exp\left(\frac{-E_{act,a}}{RT}\right) \tag{23}$$

and

$$J_{0,c} = k_c \frac{1-\varepsilon}{r_p} \exp\left(\frac{-E_{act,c}}{RT}\right) \tag{24}$$

where $E_{act,a}$ (1.0×10^5 J mol^{-1}) and $E_{act,c}$ (1.2×10^5 J mol^{-1}) are the activation energy of anode and cathode [53,54], respectively; k_a and k_c are the coefficients for exchange current density of the anode and cathode, respectively. As recommended by Chan et al. [47], the values of $J_{0,a}$ and $J_{0,c}$ at a temperature of 1073 K are equal to 5300 and 2000 A m^{-2}, respectively. Adopting these exchange current densi-

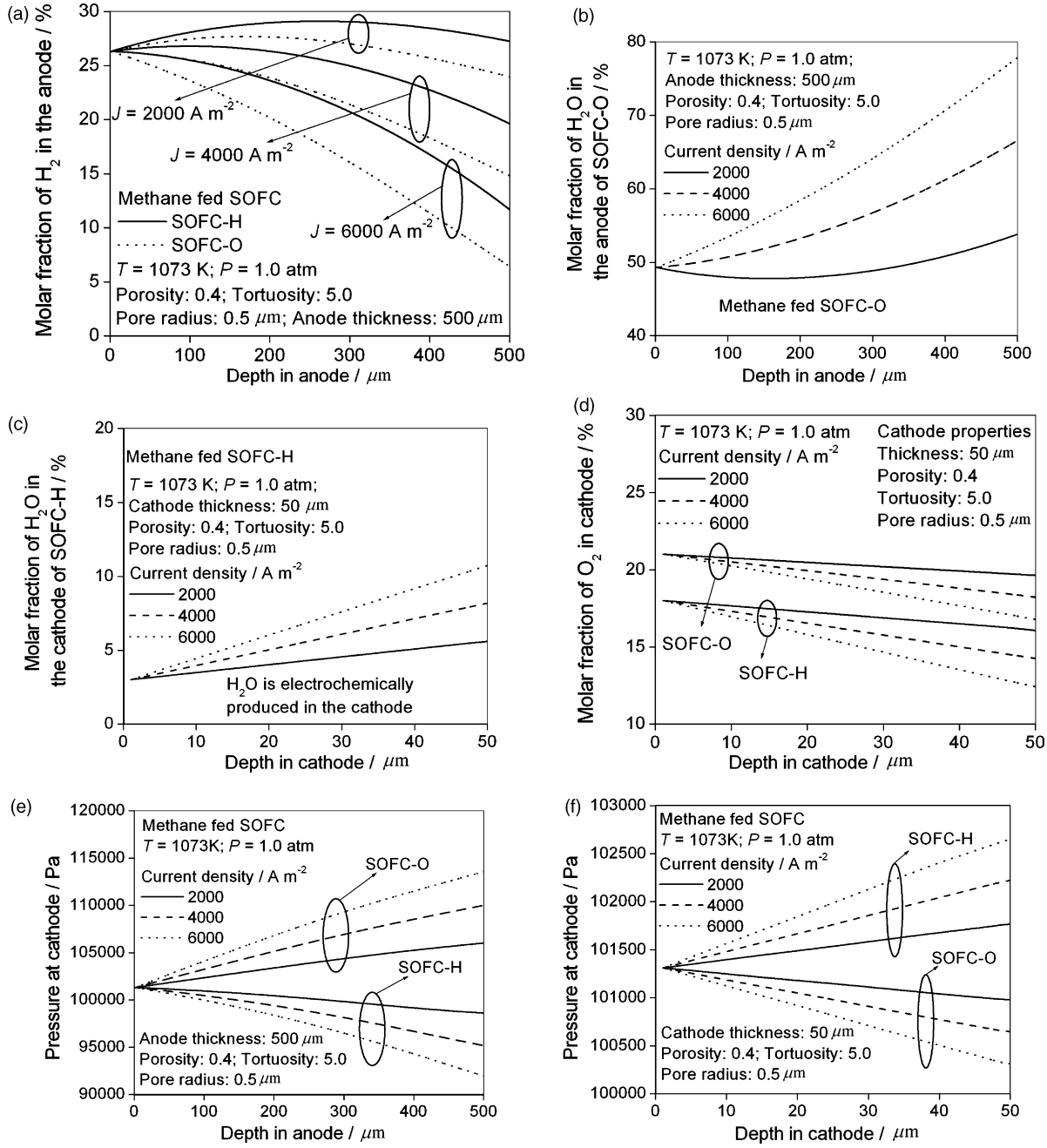

Fig. 5. Distributions of gas composition and pressure in the porous electrodes of SOFC-H and SOFC-O: (a) molar fraction of H_2 in the anode; (b) molar fraction of H_2O in the anode of SOFC-O; (c) molar fraction of H_2O in the cathode of SOFC-H; (d) molar fraction of O_2 in the cathode; (e) pressure at the anode; (f) pressure at the cathode.

ties and typical values of porosity (0.4) and pore radius (0.5 μm), the coefficients (k_a and k_c) can thus be determined from Eqs. (23) and (24).

2.1.4. Ohmic overpotential

According to Ohm's law, the ohmic overpotential of the SOFC electrolyte can be expressed in terms of the electrolyte properties by

$$\eta_{ohm} = Jd_eR_e \tag{25}$$

where d_e and R_e are the thickness and resistivity of the electrolyte, respectively. The ohmic losses at the connecting plates and electrodes are negligible compared with the ohmic loss at the electrolyte [18,47,52] and are therefore not considered in the present study.

2.2. Working potential of the CH_4 fed SOFC-O

Similar to the SOFC-H, the working potential of the CH_4 fed SOFC-O can be calculated with Eq. (3). The calculation procedures for equilibrium potential, activation overpotential, and ohmic overpotential are similar to SOFC-H. However, as H_2O is electrochemically produced in the SOFC-O anode, the mass transfer and the resulting concentration overpotentials of the SOFC-O are different from SOFC-H. Accordingly, the concentration overpotentials of the CH_4 fed SOFC-O can be expressed as

$$\eta^{O}_{conc,a} = \frac{RT}{2F}\ln\left(\frac{P^{O}_{H_2}P^{O,I}_{H_2O,a}}{P^{O,I}_{H_2}P^{O}_{H_2O,a}}\right) \tag{26}$$

$$\eta^{O}_{conc,c} = \frac{RT}{4F}\ln\left(\frac{P^{O}_{O_2}}{P^{O,I}_{O_2}}\right) \tag{27}$$

where $\eta^{O}_{conc,a}$ and $\eta^{O}_{conc,c}$ represent the concentration overpotentials of anode and cathode of the SOFC-O, respectively; $P^{O}_{H_2}$ and $P^{O,I}_{H_2}$ represent the partial pressure of H_2 at the anode surface and anode–electrolyte interface of the SOFC-O, respectively; $P^{O}_{H_2O,a}$ and $P^{O,I}_{H_2O,a}$ represent the partial pressure of H_2O at the anode surface and anode–electrolyte interface of the SOFC-O, respectively. Similarly, $P^{O}_{O_2}$ and $P^{O,I}_{O_2}$ refer to partial pressure of O_2 at the cathode surface and cathode–electrolyte interface, respectively.

Similar to the SOFC-H, molar fractions of gas species at the electrode surface of the SOFC-O are given as known boundary conditions. The fluxes at the electrode–electrolyte interface can be given as below.

In the anode:

$$N^{O}_{H_2}|_{x=d_a} = \frac{J}{2F} \tag{28}$$

$$N^{O}_{H_2O,a}|_{x=d_a} = -\frac{J}{2F} \tag{29}$$

In the cathode:

$$N^{O}_{O_2}|_{x=d_c} = \frac{J}{4F} \tag{30}$$

where $N^{O}_{H_2}$ and $N^{O}_{H_2O,a}$ are the fluxes of H_2 and H_2O in the anode; while $N^{O}_{O_2}$ is the flux of O_2 in the SOFC-O cathode.

Solving the governing equation (Eq. (14)), the concentration overpotential of the CH_4 fed SOFC-O can be obtained by substituting the interfacial (electrode–electrolyte interface) partial pressures into Eqs. (26) and (27).

3. Model evaluation

In the literature, there is no detailed experimental data on either CH_4 fed SOFC-H or CH_4 fed SOFC-O. However, there are some simulation data from literature on the CH_4 fed SOFC-O. In this section, an evaluation of the model was conducted by comparing the present modeling results with the simulation data on CH_4 fed SOFC-O from literature [55]. The typical gas composition of pre-reformed methane gas mixture was considered as the fuel for SOFC-O [55]. The working temperature and pressure were 1123 K and 1.0 atm, respectively. The thicknesses of the anode, electrolyte, and cathode were 400, 100, and 100 μm, respectively. The pore radius was 1.07 μm. The ratio of porosity to tortuosity was 0.156.

As can be seen from Fig. 2, the present simulation results agreed very well with the literature data and thus validated the present model. The difference between the present simulatioin results and Ivanov's modeling data [55] was within 5%. The discrepancy could be caused by different diffusion coefficients used. In Ivanov's study, binary diffusion coefficients at 1273 K were used to simulate the performance of the CH_4 fed SOFC-O at 1123 K. Since the diffusion coefficients increase with increasing temperature [53], Ivanov underestimated the concentration overpotentials by using higher diffusion coefficients. For comparison, temperature dependence of diffusion coefficients was fully considered in the present study as the kinetic theory of gases was used to calculate the binary diffusion coefficients [41]. Thus, the present model could predict more accurately the multi-component gas transport as well as the concentration overpotentials of the SOFC-O anode.

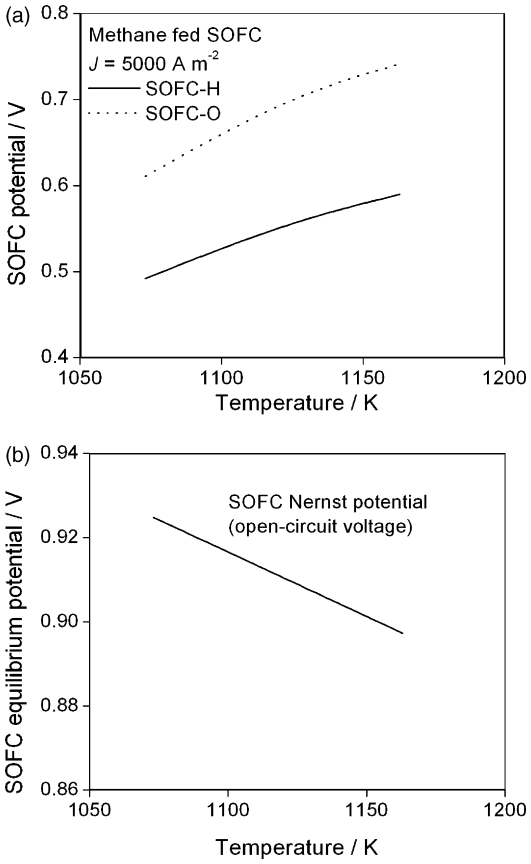

Fig. 6. Comparison of the performance of CH_4 fed SOFC-H and SOFC-H at different temperatures: (a) operating potentials of SOFC-H and SOFC-O and (b) Nernst potentials of SOFC-H.

4. Parametric analysis

The validated model was used to conduct parametric analysis to compare the performance of the CH_4 fed SOFC-H and SOFC-O. As anode support is generally the most favorable design for SOFC [44,47,48,53], the following analyses are conducted for the anode-supported SOFC-H and SOFC-O. The values of input parameters used in the parametric analysis are summarized in Table 1.

4.1. Comparison between CH_4 fed SOFC-H and SOFC-O

The complete J–V characteristics of CH_4 fed SOFC-H and SOFC-O are shown and compared in Fig. 3. As can be seen, the working potential of the CH_4 fed SOFC-H is lower than that of the SOFC-O at $J < 7500\,A\,m^{-2}$ and it quickly drops to zero at a current density of about $8600\,A\,m^{-2}$, indicating the occurrence of limiting current density. For comparison, the limiting current density for the SOFC-O is about $7500\,A\,m^{-2}$. Previous thermodynamic analyses have revealed that the theoretical performance of the CH_4 fed SOFC-H was significantly higher than the SOFC-O. However, from this study, it can be seen that the actual performance of the CH_4 fed SOFC-H is considerably lower than the SOFC-O under typical operating conditions due to its considerably higher overpotentials.

In order to identify the key sources of voltage loss, separate overpotentials of the CH_4 fed SOFC-H and SOFC-O are studied and the results are shown in Fig. 4. As expected, the ohmic overpotential of the SOFC-H is much higher than the SOFC-O, due to lower ionic conductivity of the present proton conducting materials (Fig. 4(a)). As both the SOFC-H and SOFC-O undergo similar electrochemical reactions, their activation overpotentials are identical (Fig. 4(b)).

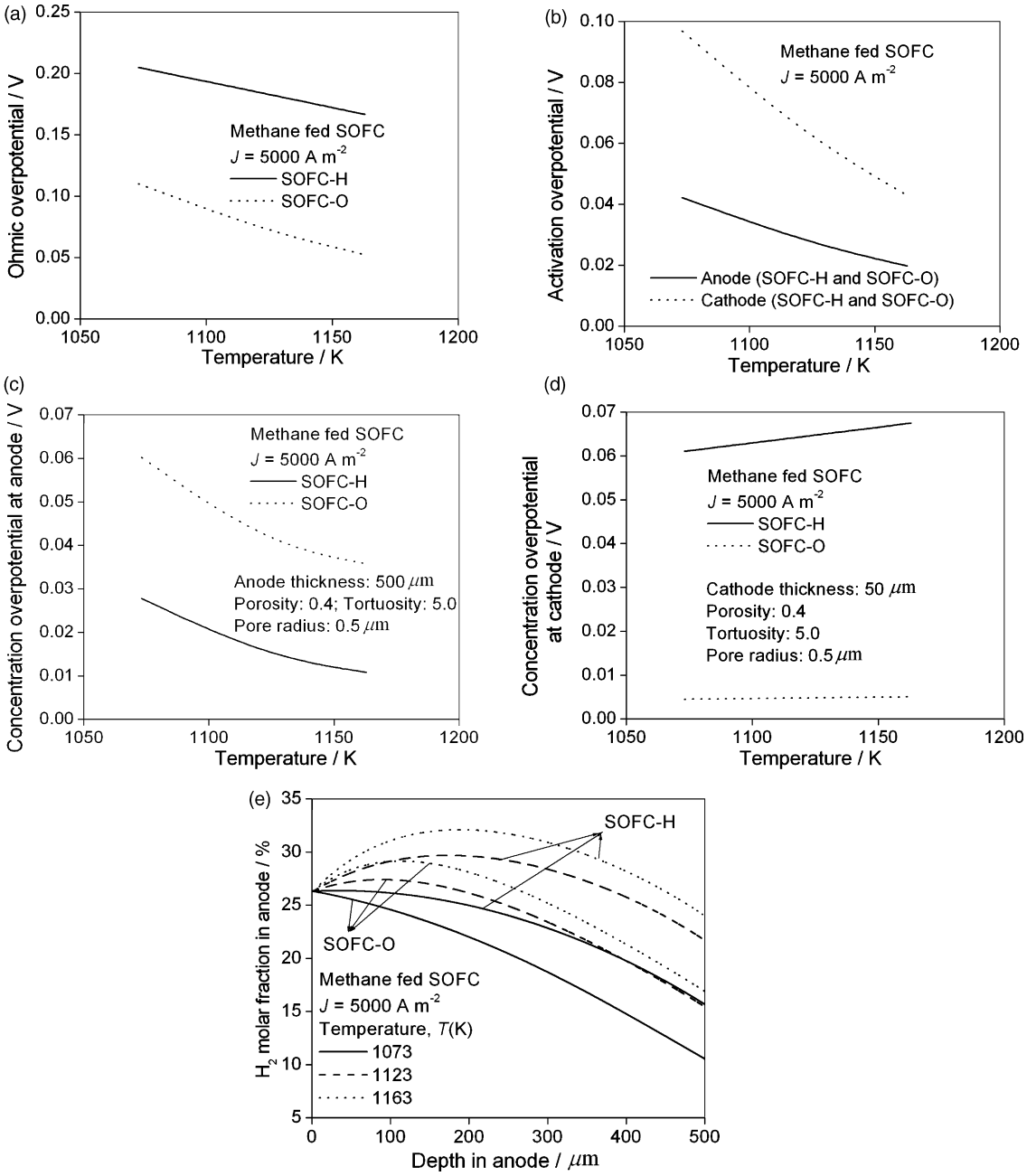

Fig. 7. Comparison of the overpotentials of CH_4 fed SOFC-H and SOFC-H at different temperatures: (a) ohmic overpotential; (b) activation overpotential; (c) anode concentration overpotential; (d) cathode concentration overpotential; (e) distribution of H_2 molar fraction in anode.

As expected, the cathode activation is found much higher than the anode activation overpotential, due to the slower electrochemical reduction of O_2 in the cathode than the reduction of H_2 at the anode.

One important finding is that the CH_4 fed SOFC-H has lower anode concentration overpotential and larger limiting current density than the SOFC-O (Fig. 4(c)). More importantly, the CH_4 fed SOFC-H is found to have much higher cathode concentration overpotential and relatively smaller limiting current density than the SOFC-O (Fig. 4(d)). In the SOFC-H, H_2O is electrochemically produced in the cathode while it is produced in the SOFC-O anode. The production of H_2O in the anode not only dilutes the concentration of H_2, but also slows down the transport of H_2 fuel from the anode surface to the TPB. Thus, the molar fraction of H_2 in the anode of the SOFC-H is higher than the SOFC-O (Fig. 5(a)). In addition, this dilution effect increases with increasing current density, leading to higher H_2O molar fraction and lower H_2 molar fraction at larger current density (Fig. 5(a)–(c)). Therefore, the use of proton conducting electrolyte is beneficial to increase the H_2 molar fraction and this is the reason that the SOFC-H has considerably higher performance than SOFC-O [56]. On the other hand, the presence of H_2O decreases the molar fraction of O_2 and impedes the transport of O_2 from the cathode surface to the TPB (Fig. 5(d)).

In addition to the gas molar fraction, the pressure distributions in the CH_4 fed SOFC-H are quite different from the SOFC-O (Fig. 5(e) and (f)). In the anode of the CH_4 fed SOFC-H, there are two competing mechanisms governing the pressure distribution: chemical reactions (MSR and WGS) and electrochemical reaction (consumption of H_2). Due to MSR, the pressure tends to increase, as the molar number of gas generation is higher than the molar number of gas consumption. Due to electrochemical reactions, H_2 is consumed in the anode while the product (H_2O) is present in the cathode of the SOFC-H, leading to lower pressure in the anode. As the chemical reaction (MSR) is insignificant at a temperature of 1073 K, the pressure decreases with anode depth in the CH_4 fed SOFC-H (Fig. 5(e)). For comparison, the electrochemical reaction does not change the pressure distribution in the CH_4 fed SOFC-O since the molar production of H_2O is equal to the molar consumption of H_2. Therefore, the pressure in the anode of the SOFC-O increases with the anode depth due to chemical reaction (MSR) (Fig. 5(e)). On the other hand, the presence of H_2O in the cathode increases the pressure in the SOFC-H cathode while the pressure decreases with cathode depth in the SOFC-O (Fig. 5(f)). The anode pressure reduction and cathode pressure increase also contribute to the lower anode concentration overpotential but higher cathode concentration overpotential of the CH_4 fed SOFC-H than the SOFC-O (Fig. 4(c) and (d)).

From the above analyses, it can be seen that the use of different electrolytes in the CH_4 fed SOFC not only cause different ionic conduction mechanisms of the electrolyte, but also cause quite different mass transfer characteristics of the porous electrodes, thus leading to considerably different concentration overpotentials and *J–V* characteristics.

4.2. Comparison between the CH_4 fed SOFC-H and SOFC-O at different operating temperatures

The SOFC performance is greatly affected by its operating and structural parameters. The following analyses are conducted under typical working conditions, i.e. a current density of 5000 A m^{-2}. The effect of operating temperature on the performance of the CH_4 fed SOFC-H and SOFC-O is shown in Fig. 6. With an increase in temperature, the working potentials of both the SOFC-H and SOFC-O are increased (Fig. 6(a)), despite of the reduction in reversible

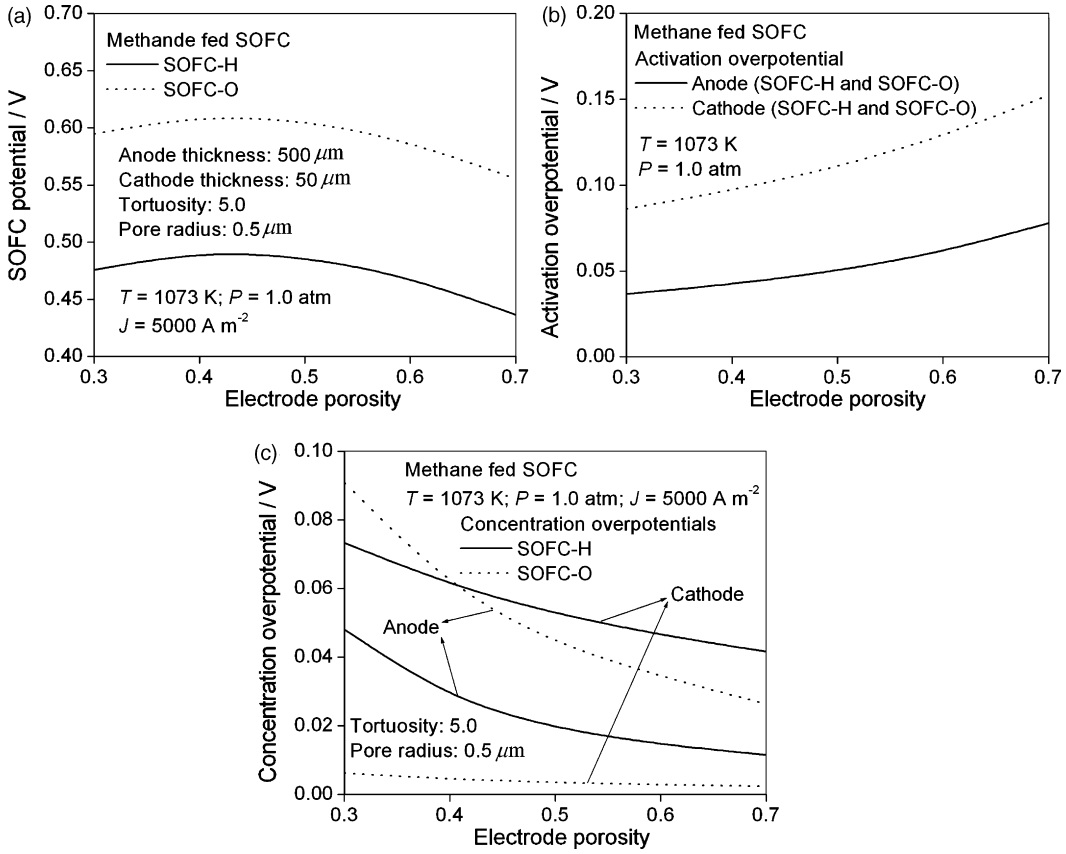

Fig. 8. Comparison of the performance of CH_4 fed SOFC-H and SOFC-O at different electrode porosity: (a) SOFC potential; (b) activation overpotential; (c) concentration overpotential.

(equilibrium) potential (Fig. 6(b)). This is because the total overpotentials decrease with increasing temperature (Fig. 7). As expected, both ohmic and activation overpotentials decrease with increasing temperature due to enhanced ionic conductivity of the electrolyte and facilitated electrochemical reactions at the TPB (Fig. 7(a) and (b)).

An interesting finding is that the anode concentration overpotentials of the CH_4 fed SOFC-H and SOFC-O are both found to decrease with increasing temperature (Fig. 7(c)). This is different from previous analysis on the H_2 fed SOFC-O, in which the electrode concentration overpotential increases with increasing temperature [57]. In the H_2 fed SOFC-O, the molar diffusion rate decreases with increasing temperature due to reduced gas density, although the effective diffusion coefficients increase with increasing temperature. As a result, the concentration overpotentials are found higher at a higher temperature. In case CH_4 is used, the MSR and WGS reactions are favored at higher temperature, leading to more H_2 production and higher H_2 molar fraction (Fig. 7(e)). Therefore, the anode concentration overpotential decreases with increasing temperature (Fig. 7(c)). However, it should be mentioned that the anode concentration overpotential does not reflect the actual mass transfer loss for the CH_4 fed SOFC. It represents the combination effect of the chemical reactions (MSR and WGS) for H_2 production and mass transfer loss. In the cathode, the concentration overpotentials are found to increase slightly with increasing temperature for both SOFC-H and SOFC-O, being consistent with previous analyses [57].

The above analysis reveals the difference between the CH_4 fed SOFC-H and SOFC-O. It can also be seen that the use of different fuels (H_2 or CH_4) can result in quite different operating mechanisms and performance characteristics.

4.3. Comparison between the CH_4 fed SOFC-H and SOFC-O with varying electrode porosity

The electrode microstructures, such as electrode porosity, pore size, and tortuosity, also influence the performance of SOFC. Fig. 8 shows the effect of electrode porosity on the CH_4 fed SOFC performance. Optimal porosities at about 0.4 are found for both the SOFC-H and SOFC-O, which minimize the working potentials (Fig. 8(a)). This is because the electrode porosity has opposite effects on activation overpotentials and concentration overpotentials. On the one hand, reducing electrode porosity can increase the length of TPB, which in turn increases the rate of electrochemical reactions and thus lower its activation overpotentials (Fig. 8(b)). On the other hand, reducing electrode porosity increases the resistance against the gas transport through the porous electrode, leading to higher concentration overpotentials (Fig. 8(c)). The combined effects of electrode porosity on activation overpotential and concentration overpotential can thus result in optimal electrode porosities. Therefore, in practice, the electrode microstructures of the SOFC need to be carefully designed to minimize the total overpotentials of the electrodes.

5. Conclusions

An electrochemical model has been developed to predict the performance of the CH_4 fed SOFC-H and SOFC-O. Comparison between the simulation results based on the present model and modeling results from literature validated the model developed in this paper.

It is found that although the CH_4 fed SOFC-H has higher theoretical performance than the SOFC-O, its actual performance is considerably lower than the SOFC-O, before the occurrence of limiting current density. The use of proton conducting electrolyte leads to significantly higher ohmic overpotential than conventional oxygen ion conducting electrolyte. In addition, the mass transfer characteristics of the SOFC-H are totally different from that of the SOFC-O, resulting in different concentration overpotentials. Although the anode concentration overpotential of the SOFC-H is found considerably lower than that of the SOFC-O, the cathode concentration overpotential of the former is remarkably higher due to the presence of H_2O in its cathode.

Increasing temperature is found beneficial to enhance working potentials of SOFC-H and SOFC-O as the total overpotentials decrease with increasing temperature. Different from previous study on the H_2 fed SOFC-O, the anode concentration overpotentials of both the CH_4 fed SOFC-H and SOFC-O are found to decrease with increasing temperature. The difference between the present and the previous study is due to the fact that H_2 is produced in the CH_4 fed SOFC via MSR and WGS. Since the rates of both the MSR and WGS increase with increasing temperature, more H_2 can be produced at elevated temperatures, and as a result, leading to higher H_2 molar fraction and lower concentration overpotentials.

There exist optimal electrode porosities that minimize the total overpotentials of the electrodes. Reducing porosity of electrodes decreases their activation overpotentials but increases their concentration overpotentials. Therefore, the microstructure of the SOFC needs to be carefully optimized to attain better performance.

The present study signifies the differences between the CH_4 fed SOFC-H and SOFC-O and provides better understanding on the working mechanisms of SOFC fed with hydrocarbon fuels. The model developed in this paper can be extended to 2D or 3D models to study the performance of actual SOFC systems.

Acknowledgements

The authors would like to thank the financial support from the CRCG of the University of Hong Kong. The authors also would like to thank Professor S.H. Chan (Nanyang Technological University, Singapore), Professor A.K. Demin (Institute of High Temperature Electrochemistry, Russia), and Professor G.Y. Meng (University of Science and Technology of China, PR China) for their valuable discussions and suggestions in this SOFC research.

References

[1] Z.P. Shao, S.M. Haile, J. Ahn, P.D. Ronney, Z.L. Zhan, S.A. Barnett, Nature 435 (2005) 795–798.
[2] T. Hibino, A. Hashimoto, T. Inoue, J. Tokuno, S. Yoshida, M. Sano, Science 288 (2000) 2031–2033.
[3] Y.H. Huang, R.I. Dass, Z.L. Xing, J.B. Goodenough, Science 312 (2006) 254–257.
[4] S.H. Chan, C.F. Low, O.L. Ding, Journal of Power Sources 103 (2002) 188–200.
[5] J.J. Hwang, C.K. Chen, D.Y. Lai, Journal of Power Sources 143 (2005) 75–83.
[6] J.L. Yuan, M. Rokni, B. Sunden, International Journal of Heat and Mass Transfer 46 (2003) 809–821.
[7] Y.X. Lu, L. Schaefer, P.W. Li, Journal of Power Sources 140 (2005) 331–339.
[8] P.W. Li, M.K. Chyu, Journal of Power Sources 124 (2003) 487–498.
[9] M.M. Husain, X. Li, I. Dincer, Journal of Power Sources 161 (2006) 1012–1022.
[10] M. Granovskii, I. Dincer, M.A. Rosen, Journal of Power Sources 165 (2007) 307–314.
[11] R. Suwanwarangkul, E. Croiset, M.D. Pritzker, M.W. Fowler, P.L. Douglas, E. Entchev, Journal of Power Sources 154 (2006) 74–85.
[12] W.G. Bessler, S. Gewies, M. Vogler, Electrochimica Acta 53 (2007) 1782–1800.
[13] D. Ding, W. Zhu, J.F. Gao, C.R. Xia, Journal of Power Sources 179 (2008) 177–185.
[14] M. Ni, M.K.H. Leung, D.Y.C. Leung, Journal of Power Sources 168 (2007) 369–378.
[15] V.M. Janardhanan, V. Heuveline, O. Deutshmann, Journal of Power Sources 172 (2007) 296–307.
[16] H. Zhu, R.J. Kee, V.M. Janardhanan, O. Deutschmann, D.G. Goodwin, Journal of the Electrochemical Society 152 (2005) A2427–A2440.
[17] S.C. Singhal, K. Kendall, High-temperature Solid Oxide Fuel Cells: Fundamentals Design and Applications, Elsevier Science, Oxford, 2003.
[18] J.R. Ferguson, J.M. Fiard, R. Herbin, Journal of Power Sources 58 (1996) 109–122.
[19] R. Bove, S. Ubertini, Journal of Power Sources 159 (2006) 543–559.

[20] D. Cui, L. Liu, Y.L. Dong, M.J. Cheng, Journal of Power Sources 174 (2007) 246–254.
[21] S.H. Chan, O.L. Ding, International Journal of Hydrogen Energy 30 (2005) 167–179.
[22] E.S. Hecht, G.K. Gupta, H.Y. Zhu, A.M. Dean, R.J. Kee, L. Maier, O. Deutschmann, Applied Catalysis A: General 295 (2005) 40–51.
[23] G.K. Gupta, A.M. Dean, K.Y. Ahn, R.J. Gorte, Journal of Power Sources 158 (2006) 497–503.
[24] V.M. Janardhanan, O. Deutschmann, Journal of Power Sources 162 (2006) 1192–1202.
[25] N. Laosiripojana, S. Assabumrungrat, Journal of Power Sources 163 (2007) 943–951.
[26] M. Ni, M.K.H. Leung, D.Y.C. Leung, Journal of Power Sources 177 (2008) 369–375.
[27] M. Ni, M.K.H. Leung, D.Y.C. Leung, Fuel Cells 7 (2007) 269–278.
[28] G.Y. Meng, G.L. Ma, Q.L. Ma, R.R. Peng, X.Q. Liu, Solid State Ionics 178 (2007) 697–703.
[29] A. Wojcik, H. Middleton, I. Damopoulos, J. Van herle, Journal of Power Sources 118 (2003) 342–348.
[30] Q.L. Ma, R.R. Peng, Y.J. Lin, J.F. Gao, G.Y. Meng, Journal of Power Sources 161 (2006) 95–98.
[31] L.M. Zhang, W.S. Yang, Journal of Power Sources 179 (2008) 92–95.
[32] A. Demin, P. Tsiakaras, International Journal of Hydrogen Energy 26 (2001) 1103–1108.
[33] A.K. Demin, P.E. Tsiakaras, V.A. Sobyanin, S.Y. Hramova, Solid State Ionics 152/153 (2002) 555–560.
[34] S. Assabumrungrat, W. Sangtongkitcharoen, N. Laosiripojana, A. Arpornwichanop, S. Charojrochkul, P. Praserthdam, Journal of Power Sources 148 (2005) 18–23.
[35] W. Jamsak, S. Assabumrungrat, P.L. Douglas, N. Laosiripojana, S. Charojrochkul, Chemical Engineering Journal 119 (2006) 11–18.
[36] S. Assabumrungrat, N. Laosiripojana, P. Piroonlerkgul, Journal of Power Sources 159 (2006) 1274–1282.
[37] W. Jamsak, S. Assabumrungrat, P.L. Douglas, N. Laosiripojana, R. Suwanwarangkul, S. Charojrochkul, E. Croiset, Chemical Engineering Journal 133 (2007) 187–194.
[38] Y. Matsuzaki, I. Yasuda, Journal of the Electrochemical Society 147 (2000) 1630–1635.
[39] A.M. Sukeshini, B. Habibzadeh, B.P. Becker, C.A. Stoltz, B.W. Eichhorn, G.S. Jackson, Journal of the Electrochemical Society 153 (2006) A705–A715.
[40] V.M. Janardhanan, O. Deutschmann, Chemical Engineering Science 62 (2007) 5473–5486.
[41] M. Ni, M.K.H. Leung, D.Y.C. Leung, Chemical Engineering & Technology 29 (2006) 636–642.
[42] W. Lehnert, J. Meusinger, F. Thom, Journal of Power Sources 87 (2000) 57–63.
[43] R. Suwanwarangkul, E. Croiset, M.W. Fowler, P.L. Douglas, E. Entchev, M.A. Douglas, Journal of Power Sources 122 (2003) 9–18.
[44] M. Ni, M.K.H. Leung, D.Y.C. Leung, Chemical Engineering & Technology 30 (2007) 587–592.
[45] M. Ni, M.K.H. Leung, D.Y.C. Leung, Journal of Power Sources 163 (2006) 460–466.
[46] M. Ni, M.K.H. Leung, D.Y.C. Leung, Electrochimica Acta 52 (2007) 6707–6718.
[47] S.H. Chan, K.A. Khor, Z.T. Xia, Journal of Power Sources 93 (2001) 130–140.
[48] F. Barbir, PEM Fuel Cells—Theory and Practice, Elsevier Academic Press, 2005, pp. 36–39.
[49] E.S. Greene, W.K.S. Chiu, M.G. Medeiros, Journal of Power Sources 161 (2006) 225–231.
[50] X.J. Chen, S.H. Chan, K.A. Khor, Electrochimica Acta 49 (2004) 1851–1861.
[51] J.H. Nam, D.H. Jeon, Electrochimica Acta 51 (2006) 3446–3460.
[52] P. Costamagna, P. Costa, V. Antonucci, Electrochimica Acta 43 (1998) 375–394.
[53] E. Hernandez-Pacheco, M.D. Mann, P.N. Hutton, D. Singh, K.E. Martin, International Journal of Hydrogen Energy 30 (2005) 1221–1233.
[54] P. Costamagna, A. Selimovic, M.D. Borghi, G. Agnew, Chemical Engineering Journal 102 (2004) 61–69.
[55] P. Ivanov, Electrochimica Acta 52 (2007) 3921–3928.
[56] M. Ni, D.Y.C. Leung, M.K.H. Leung, Journal of Power Sources, in press.
[57] M. Ni, M.K.H. Leung, D.Y.C. Leung, Energy Conversion and Management 48 (2007) 1525–1535.